



Continuous Synthesis of Glycerol Carbonate by Transesterification of Glycerol with Dimethyl Carbonate Over Fe–La Mixed Oxide Catalysts

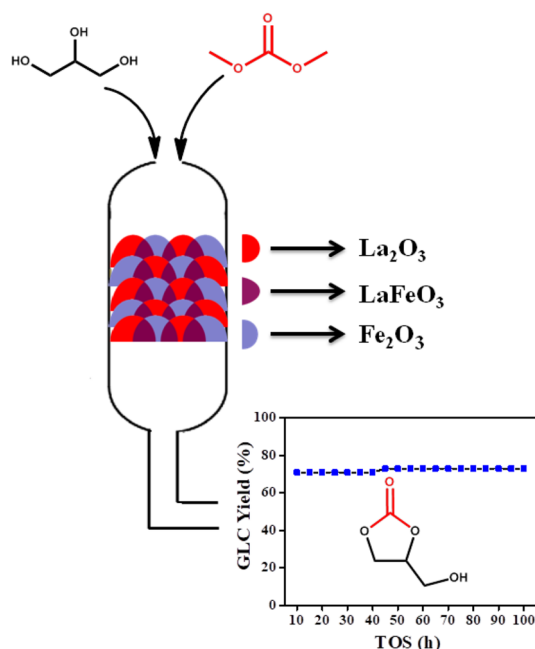
Piyusa P. Pattanaik^{1,2} · P. Mahesh Kumar^{1,2} · N. Raju¹ · N. Lingaiah^{1,2}

Received: 16 June 2020 / Accepted: 17 September 2020
© Springer Science+Business Media, LLC, part of Springer Nature 2020

Abstract

Transesterification of glycerol with dimethyl carbonate to produce glycerol carbonate was studied under continuous reaction over Fe–La mixed oxide catalysts. A series of Fe–La oxide catalysts with different molar compositions were synthesized by co-precipitation method. Surface and structural investigations of the catalysts were carried using N₂ physisorption, powder X-ray diffraction, temperature-programmed desorption, X-ray photoelectron spectroscopy, FT-infra red spectroscopy, scanning electron microscopy and Laser Raman spectroscopy. Glycerol carbonate yield was influenced by the molar ratios of Fe/La and catalyst calcination temperature, which are responsible for the variation in acid–base properties of the catalysts. The catalyst with a molar ratio of 1:1 calcined at 550 °C exhibited superior activity with 71% yield of glycerol carbonate. The synergistic effect between Fe–La oxides and the formation of LaFeO₃ perovskite structure are responsible for the high activity of the catalyst. The catalyst exhibited unprecedented stability over 100 h during the time on stream analysis.

Graphic Abstract



Keywords Glycerol · Dimethyl carbonate · Glycerol carbonate · Fe–La mixed oxides · Transesterification

Electronic supplementary material The online version of this article (<https://doi.org/10.1007/s10562-020-03397-4>) contains supplementary material, which is available to authorized users.

Extended author information available on the last page of the article

1 Introduction

The increasing worldwide demand for biofuels could retard the harmful effect on the environment like greenhouse gas emissions occurring from the burning of fossil fuels [1–3]. Among the biofuels, biodiesel is a green and sustainable fuel in place of petroleum diesel [4]. The high production of biodiesel could obviously resolve the future energy crisis in society. The preparation of biodiesel from vegetable oils by transesterification led to generate about ten percent of glycerol as a by-product. Glycerol, a highly functional molecule is a useful platform chemical to prepare different value-added products. It can be converted into various useful chemicals by different chemical transformation reactions such as hydrogenolysis, esterification, oxidation, carbonylation, etc. to synthesize chemicals like 1,2-propanediol, acrolein, esters of glycerol and glycerol carbonate (GLC) etc. [5–7].

Among the different possible products from glycerol, GLC is one of the important molecules as it has extensive applications in the preparation of polymers like polyesters, polycarbonates, polyurethanes, surfactants, coatings, adhesives, and lubricants [8–10]. It is widely used also as a green solvent due to its low volatility and nontoxic nature.

Various routes for the synthesis of GLC from glycerol were practiced. Synthesis of GLC largely carried by phosgene and oxidative carbonylation routes. These routes are having strong limitations due to the toxic nature of the reactants [11]. Another method for the preparation of GLC is direct carbonylation of glycerol with CO₂. This approach is not gained importance because of low yield and requires supercritical conditions [12, 13]. Alcoholysis of urea for GLC synthesis by fixing CO₂ during urea preparation may be an effective way but have a fair limitation since the reaction should carry under reduced pressure conditions for removing ammonia continuously.

A productive and promised pathway for synthesis of GLC is the transesterification of glycerol with dimethyl carbonate (DMC) [14, 15]. The synthesis of GLC by transesterification was mainly achieved using base catalysts. Several base catalysts like NaOH, KOH and K₂CO₃, etc. were studied under homogeneous conditions. The separation and reusability of the catalysts are the major drawbacks for these catalysts even though the activity is very high [16]. On the other hand, heterogeneous solid base catalysts that overcome all these limitations are studied extensively. Different catalytic systems such as alkali and alkaline earth metal oxides, hydrotalcite, mixed base oxides have been studied for the preparation of GLC from glycerol and DMC [17, 18]. Most of these catalysts showed reasonable activity and these reactions are carried in batch process. Some of these catalysts showed limited activity upon reuse.

Nowadays the continuous process is gaining importance in the synthesis of fine chemicals as this approach overcomes

the limitations associated with the batch process. The preparation of GLC by continuous transesterification reaction will be more advantageous compared to the batch process. In the batch process, the formation of consecutive products like glycidol is possible at high glycerol conversion. The continuous reaction for GLC preparation will lead to selective formation of the desired product with high throughput.

In recent times few studies reported for the synthesis of glycerol carbonate in continuous mode [19–23]. Lari et al. reported hydrotalcite mixed oxide catalysts using urea as the source of carbonylation where the highest 60% yield of GLC obtained using the aprotic solvent and catalytic binder. The catalytic deactivation found after 10–15 h and the yield lowered to 20% at the end of the reaction [24]. Wang et al. recently reported modified organocatalyst P₂-tBu/PS as the heterogeneous catalyst using DMC as the source of carbonylation under continuous reaction. It has been found a gradual decrease in catalytic activity after 3 h and dropped to 15% less in conversion by the end of 33 h of the reaction [22]. Even though few researchers attempted continuous reaction for the preparation of GLC, the overall activity and stability are limited. The main drawback glycerol carbonate synthesis during continuous operation is the stability of the base catalysts. Development of stable catalyst is essential for the preparation of glycerol carbonate from glycerol transesterification under environmentally benign continuous process in place of existing batch process. It has been reported that lanthanum oxide containing mixed oxides showed better catalytic performance in transesterification of glycerol [25, 26]. La in combination with other metal oxide like Mg, Zn are explored as base catalysts for transesterification reaction with high stability [27]. It is thought the addition of La to Fe oxide may improve the basicity and stability of the catalyst towards the transesterification of glycerol with DMC.

The current work discloses the preparation of Fe and La mixed oxide catalysts for the selective transesterification of glycerol with DMC under continuous reaction conditions. Mixed oxides of Fe and La were prepared with different molar ratios and assessed for continuous transesterification of glycerol under moderate reaction conditions. The reaction was studied at different conditions to optimize the maximum yield. The establishment of the stability of the catalysts is one of the aims of the present study.

2 Experimental

2.1 Materials

Glycerol (GLY: ≥ 99% pure) was procured from Fisher Scientific, India. The metal precursors, La(NO₃)₃·6H₂O and Fe(NO₃)₃·9H₂O obtained from Merck Chemicals, India.

Dimethyl carbonate was purchased from Finar Chemicals Ltd. All chemicals were used without further purification.

2.2 Catalysts Preparation

Fe and La mixed oxide catalysts were prepared by co-precipitation method with varying their molar ratios. In a typical procedure, the required calculated amount of $\text{Fe}(\text{NO}_3)_3$ and $\text{La}(\text{NO}_3)_3$ were dissolved in deionized water. The solution was precipitated by adding a dilute ammonia solution drop by drop while stirring. The addition of ammonia solution continued until the pH of the solution reaches 10. Further, the stirring was continued for 30 min. After that, the slurry was kept for aging at 60 °C over a period of 6 h with vigorous stirring. Then the solution was washed thoroughly with distilled water and then the residue was dried overnight at 100 °C in an air oven. The obtained solid mass was thermally calcined in static air at 450–850 °C for 4 h with a ramping rate of 5 °C/min to obtain Fe–La catalysts. Fe–La mixed oxide catalysts with molar ratios of 1:1, 1:2, 1:3, 2:1 and 3:1 were prepared and labelled as FL-11, FL-12, FL-13, FL-21, and FL-31 catalysts. The F and L correspond to Fe and La and the numbers indicate the respective molar ratio.

2.3 Catalyst Characterization

The structural characteristics of the catalysts were determined using an X-ray diffractometer which operated at a specific tube voltage of 40 kV and tube current of 30 mA equipped with Ni-filtered $\text{CuK}\alpha$ source. The diffractograms were recorded at a 2-theta range of 10°–80° with angular steps of 0.0450° and step time of 0.7 s.

The surface area of the catalysts was estimated using the N_2 physisorption method over BELSORP II (BEL Japan. Inc.) instrument. Prior to analysis about 0.2 g of the sample was subjected to vacuum to outgas the surface at 200 °C for 2 h. The N_2 adsorption isotherm was measured and the surface area was calculated using the BET equation. FT-IR analyses of the samples were obtained on a DIGILAB Bio-rad spectrometer using KBr disc at a resolution of 1 cm^{-1} . Scanning electron microscopy analysis were performed using JEOL FE-SEM-7610F microscope to elucidate the morphology. Thermo gravimetric analysis (TGA) was performed on TGA Q500 V20.13 Build 39 instrument.

The basicity and basic site strength of the catalysts were estimated by temperature-programmed desorption of CO_2 . About 0.1 g of the solid sample was taken in the quartz sample tube and pre-treated at 300 °C for 60 min in inert condition to remove impurities over the catalyst surface. Then the sample was cooled and allowed for adsorption of 10% CO_2 balance He at room temperature. Then the surface of the catalyst was made free from the physisorbed CO_2 through purging with He gas over the catalyst surface. After that

desorption of CO_2 was carried by increasing the temperature up to 800 °C with a temperature ramp of 10 °C/min and the desorbed CO_2 was estimated. Similarly, the acidic sites and strength of the catalysts were measured from the temperature desorption of NH_3 where the aforementioned pre-treatment and analysis conditions were similar except the adsorption of 5% NH_3 balance He gas at 100 °C as the probe molecule in place of CO_2 .

The elemental composition of the catalysts quantified by X-ray fluorescence spectroscopy (XRF) operated at 35 kV using the Rh source. The catalysts were characterized by Raman spectroscopy (Horiba Jobin–Yvon Lab Ram HR, Japan) using 633 nm He–Ne laser. The spectra were recorded by spreading about 10 mg of solid sample over a glass slide kept under microscope.

The oxidation state and presence of anionic vacancies of the catalysts were acquired from the binding energy of the element using the XPS analysis. The spectra were obtained using the AXIS Nova spectrometer. The quantitative parallel imaging of the catalysts was recorded with a 165 mm radius hemispherical analyser and a spherical mirror analyzer coupled with a Delay-line detector. The non-monochromatic $\text{Mg K}\alpha$ X-ray using a dual anode of Mg and Al (1486.6 eV) which was controlled by 12.5 kV and 16 mA. Prior to analysis, the sample was degassed at 100 °C under vacuum (1×10^{-7} Torr) for 3 h for cleaning catalyst surface. The instrument was calibrated by using Au as standard and the energy calibration was made by C (1s) photoelectron using the binding energy of 284.6 eV. Also, the charge neutralization of 2 eV balanced to charge up the sample.

2.4 Continuous Transesterification of Glycerol

The continuous transesterification of glycerol with DMC was carried in a fixed bed downflow reactor at atmospheric pressure. In this procedure, about 1 g of catalyst diluted with equal amount of quartz particles and was suspended in the reactor under isothermal zone with the help of two quartz wool plugs. The catalyst was pre-treated under N_2 gas atmosphere at 450 °C for 1 h. After that, the temperature of the catalyst bed was brought to the required reaction temperature. The reaction was conducted by passing the reactants glycerol and DMC with two dosing pumps along with N_2 as the carrier gas. The reaction was carried in the temperature range of 200–260 °C. The products coming out of the reactor were collected in a trap kept undercooling. The products were quantified by analysing gas chromatography (Shimadzu 2010 plus, Japan) equipped with flame ionization detector by separating the products over a capillary column (Innowax, diameter: 0.25 mm, length: 30 m). The yield of the product was estimated by using the following equation.

$$\text{Yield}(\%) = \frac{\text{Conversion of Glycerol} \times \text{Selectivity of Glycerol Carbonate}}{100}$$

$$\text{Rate}_{\text{GLY}} = \frac{\text{Yield of Glycerol carbonate} \times \text{Feed Rate (mmol/s)}}{\text{gm of catalyst (gcat)}}$$

3 Results and Discussion

3.1 Catalysts Characterization

The elemental composition and surface properties of the Fe–La mixed oxide catalysts are shown in Table 1. It has been found that the FL-11 catalyst exhibited a surface area of 16.4 m²/g. Further increase in La content (FL-12 and FL-13 catalysts) surface area increased marginally. On the other hand, increasing the Fe content (FL-21 and FL-31 catalysts) the surface area increased substantially up to 53.8 m²/g. However, further, increase in Fe content (FL-31 catalyst) a marginal decrease in surface area to 45.4 m²/g was noticed. Thus, it has been inferred that the incorporation of Fe resulted in improvement in the surface area to a higher value [28].

The results indicate that variation in the content of Fe or La affected the surface area of the Fe–La mixed oxide catalysts.

Fe–La oxide catalysts are characterized by X-ray diffraction and the patterns are shown in Fig. 1. The diffraction peaks of La₂O₃ (JCPDS 74-2430) found in bulk La₂O₃ and Fe–La mixed oxides at diffraction angles of 26.02° 29.72° and 55.25° which corresponding to the hexagonal phase of La₂O₃ having lattice planes of (100), (101) and (200) respectively. The absence of Fe₂O₃ diffraction peaks in Fe–La mixed oxides might be due to good interaction of the host oxide. Apart from these, diffraction peaks related to La₂O₂CO₃ (JCPDS 84-1964) and La(OH)₃ (JCPDS 83-2034) phases were observed for bulk La₂O₃ [25, 29]. The mixed oxide catalysts showed the presence of LaFeO₃ phase in

all the catalysts as a major phase. FL-11 catalyst exhibited peaks at 32.34°, 39.86°, 46.36°, 52.08°, 57.61°, 67.62°, and 76.70° are attributed to LaFeO₃ phase (JCPDS 88-0641). At the equimolar content of Fe and La, the insertion of Fe₂O₃ into the lattice of La₂O₃ might take place to form a predominantly LaFeO₃ phase [30]. Upon increasing the Fe content (FL-21 catalyst) significant formation of La₂O₂CO₃ occurred while further increase in Fe (FL-31 catalyst) diminished La₂O₂CO₃ species in the mixed oxides due to enhanced cationic mobility of Fe³⁺ ions [31].

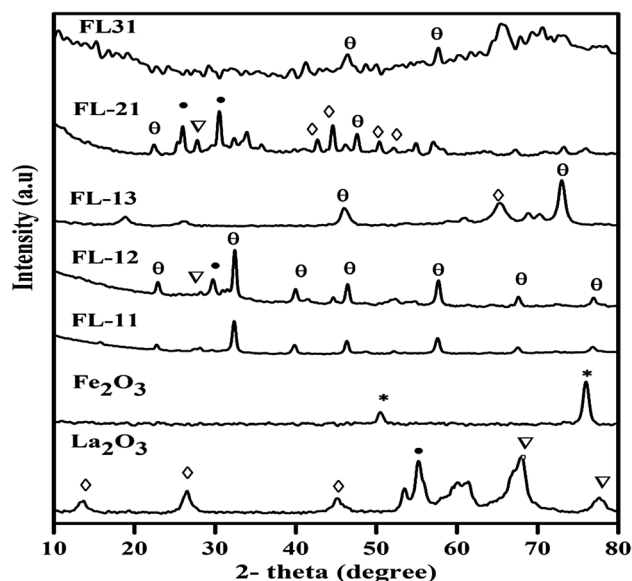


Fig. 1 Powder XRD patterns of Fe–La mixed oxide catalysts. La₂O₃ (filled circle), La(OH)₃ (inverted triangle), Fe₂O₃ (asterisk), La₂O₂CO₃ (open diamond) and LaFeO₃ (theta)

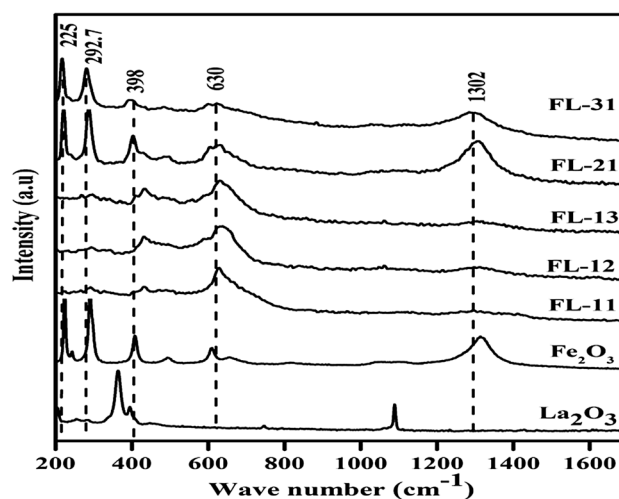


Fig. 2 Raman spectra of Fe–La mixed oxide catalysts

Table 1 Composition and surface properties of Fe–La mixed oxide catalysts

S. no.	Catalyst	Fe content ^a	La content ^a	Surface area (m ² /g)
1	FL11	0.97	1.03	16.4
2	FL12	0.89	2.11	17.9
3	FL13	1.06	2.94	22.4
4	FL21	1.92	1.08	53.8
5	FL31	3.04	0.96	45.3

^aMolar content measured from XRF analysis.

Raman spectra of Fe–La mixed oxide catalysts are shown in Fig. 2. Pure La_2O_3 catalyst showed the characteristic Raman bands at 363.6, 394.5 and 1090 cm^{-1} . Fe_2O_3 catalyst exhibited bands at 225, 292.6, 409, 496.08, 609.7, 656.07, and 1314.8 cm^{-1} which are due to the presence of $\alpha\text{-Fe}_2\text{O}_3$ in hematite phase [32, 33]. The mixed oxide FL catalysts showed the major band at 630 cm^{-1} related to the LaFeO_3 phase. This phase is observed in the catalysts with an equal or high molar ratio of La (FL-11, 12 and 13 catalysts). These catalysts did not show the bands related to individual oxides. These results indicate that the mixed oxide phase is predominant in these catalysts. The catalysts with high Fe content (FL-21 and 31) showed the Raman bands related to the Fe_2O_3 phase apart from LaFeO_3 mixed oxide. The presence of the hematite phase is responsible for lowering the formation of $\text{La}_2\text{O}_2\text{CO}_3$ species by the mobility of Fe^{3+} over the catalyst surface [30].

The FL catalysts are characterized by FT-IR spectroscopy and the spectra are depicted in Fig. S1 (Supplementary information). The FL catalysts with 1:1, 1:2, 1:3 molar ratio showed a peak around 595 cm^{-1} . This was attributed to the stretching mode vibration involving internal motion during change in the length of Fe–O or Fe–O–Fe bond. This is the characteristic band of octahedral FeO_6 group in LaFeO_3 structure [34]. The absorption bands appeared at 1644 and 1360 cm^{-1} were assigned to the interaction between atmospheric CO_2 and LaFeO_3 phase, which suggested the formation of La–carbonate species on the LaFeO_3 surface [35]. The broad absorption peaks observed in the range of $1400\text{--}1500\text{ cm}^{-1}$ belonging to the absorption peaks of water/surface hydroxyl on the LaFeO_3 crystal surface. The FT-IR results are in support of the observations made from Raman spectroscopy about the presence of LaFeO_3 phase in $\text{Fe}_2\text{O}_3\text{--La}_2\text{O}_3$ mixed oxide catalysts.

The representative FL-11 catalyst is characterized by XPS. The XPS spectra of Fe, La, and O_2 of FL-11 catalyst are shown in Fig. 3. It showed the B.E values related to Fe $2p_{3/2}$ and $2p_{1/2}$ at 710 and 723 eV along with satellite peaks at 718 and 732 eV respectively [32]. It has been reported that the presence of satellite peaks is usually observed right after $\sim 8\text{ eV}$ of parent peak which confirms the existence of Fe in +3 oxidation state [33, 36, 37]. The binding energy at 833.5 and 837 eV are ascribed to $\text{La } 3d_{5/2}$ and the binding energy at 850 and 854 eV corresponds to $\text{La } 3d_{3/2}$ with the splitting of about 4.5 eV corresponds to La_2O_3 with La in +3 oxidation state [38]. The existence of Fe–O and La–O bond confirmed by the availability of core oxygen at a binding energy of 530 eV which is related to lattice oxygen (O_L) in anionic vacancy and possible to form mixed oxide (Fe–La–O) structure of the catalyst [38]. The binding energy at 538 eV was observed which is attributed to the physisorbed molecular oxygen (O_M) [39].

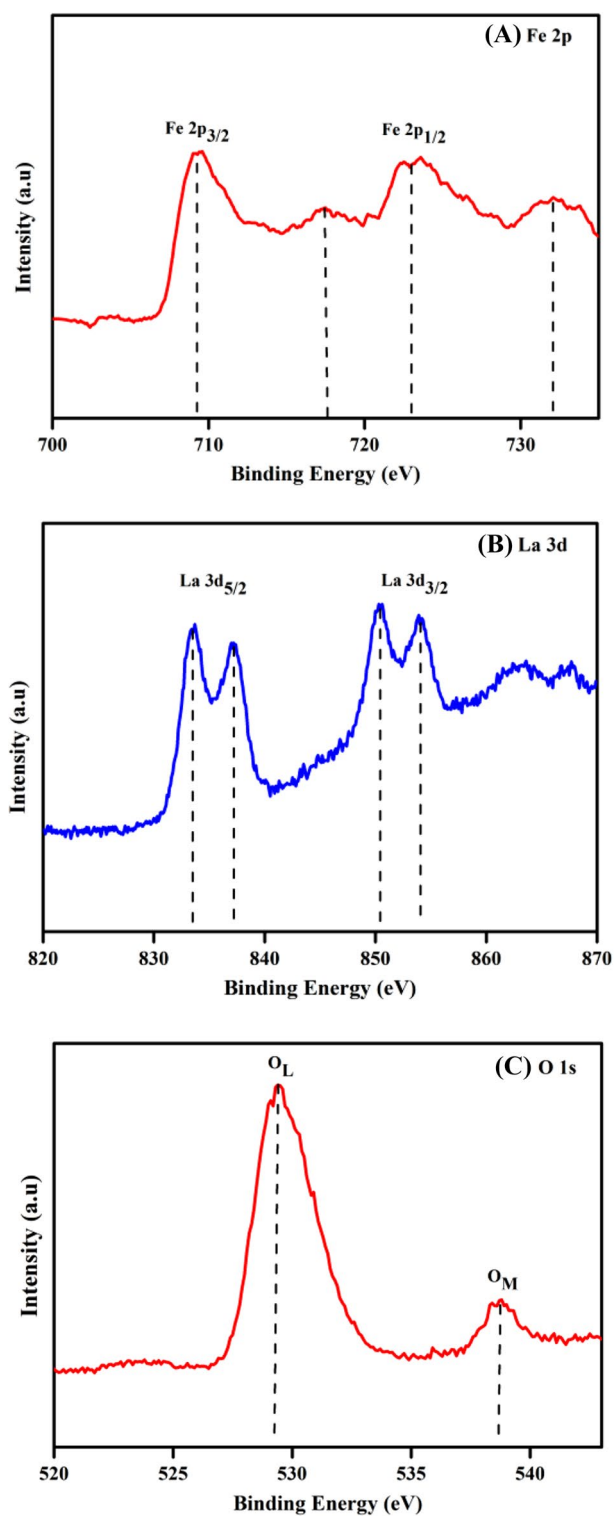


Fig. 3 XPS spectrum of FL-11 catalyst a Fe 2p, b La 3d and c O 1s

The basicity of Fe–La mixed oxide catalysts was analysed by TPD of CO_2 and the results are shown in Table 2. All the catalysts showed a desorption peak at high temperature centred at around $750\text{ }^\circ\text{C}$ related to strong basic sites as

Table 2 Acid–base properties of Fe–La mixed oxide catalysts

S. no.	Catalyst	Basicity (mmol/g)	Acidity (mmol/g)
1	FL11-550	1.41	0.382
2	FL12-550	0.315	0.350
3	FL13-550	0.755	0.845
4	FL21-550	0.737	0.634
5	FL31-550	0.228	0.161

shown in Fig. S2 (Supplementary information). Among all the FL-11 catalyst showed high basicity of 1.41 mmol/g. The high basicity of the FL-11 catalyst might be due to the presence of mixed oxide LaFeO₃ phase.

FL catalysts acidity was determined by TPD of NH₃ and the results are presented in the same Table along with basicity. The patterns suggest that the catalysts are possessing strong acidic sites apart from few moderate acidic sites as shown in Fig. S3 (Supplementary information). The total acidity of the catalysts is estimated by calculating the area of the desorption peaks. The results indicate that an increase in La content in the catalysts enhanced the total acidity. However, increasing Fe content in the catalysts resulted in lower acidity. The TPD of both CO₂ and NH₃ results directly confirms that the FL catalysts are posing both acid and base properties.

3.2 Glycerol Transesterification Activity

The continuous transesterification of glycerol with DMC was carried over FL mixed oxide catalysts and the results are illustrated in Table 3. The activity results of the bulk La₂O₃ and Fe₂O₃ catalysts were included for the sake of comparison. The catalysts showed near complete selectivity to glycerol carbonate. The bulk La₂O₃ and Fe₂O₃ catalysts exhibited 49% and 53% yield of GLC respectively. The FL-11 catalyst exhibited the highest GLC yield of 71%.

On increasing the La composition in the catalyst (FL-12 and FL-13 catalysts), a gradual decrease in activity was

Table 3 Activity data of the Fe–La mixed oxide catalysts during continuous glycerol transesterification

Sl. no.	Catalysts	GLC yield (%)
1	Fe ₂ O ₃	53
2	La ₂ O ₃	49
3	FL-11	71
4	FL-12	53
5	FL-13	60
6	FL-21	51
7	FL-31	48

noticed. However, the catalytic activity marginally increased upon increasing the Fe molar composition (FL-21 and FL-31 catalysts). The catalytic activity of the catalysts are as follows: FL-11 > FL-13 > FL-12 > FL-21 > FL-31. Thus, it is evident that the equimolar composition of La₂O₃ and Fe₂O₃ (FL-11 catalyst) in the catalyst resulted in the enhanced activity. The variation of the FL catalysts activity can be correlated with their surface-structural and acid–base properties. The FL-11 catalyst showed the presence of both strong basic and acid sites. This catalyst also contains the mixed oxide LaFeO₃ perovskite phase which account for the presence of La³⁺ and Fe³⁺ in the cationic lattice and O²⁻ anionic lattice as revealed from XPS analysis. Raman spectra of the FL-11 catalyst also indicated the existence of the LaFeO₃ phase.

The acid–base sites play an important role in the transesterification reaction of glycerol with DMC. The hydroxyl groups of glycerol are adsorbed on basic sites of the catalysts by hydrogen bonding. The other reactant DMC is activated on acidic sites of the catalyst. The activated hydroxyl group undergoes nucleophilic attack on the carbonyl group of DMC leading to the formation of glycerol-DMC adduct by the elimination of methanol. Then the active hydroxyl groups and carbonyl groups of the adduct undergoes an intramolecular nucleophilic substitution with the elimination of another methanol molecule to give glycerol carbonate [40]. The high activity of the FL-11 catalyst might be due to the presence of high amount of both basic and acidic sites.

3.3 Influence of Catalyst Calcination Temperature on Transesterification Activity

Along with the metal oxide content in the catalyst, the calcination temperature has a strong influence over the surface and structural properties of the catalysts. The active FL-11 catalyst was calcined at different calcination temperatures in the range of 450–750 °C and evaluated for their activity towards glycerol carbonate preparation. The activity of the catalyst is shown in Table 4. The GC yield increased from 56 to 71% with enhancement in calcination temperature from 450 to 550 °C. Further increasing the calcination

Table 4 Glycerol transesterification activity of FL-11 catalyst calcined at different temperatures

S. no.	Catalyst	Calcination temperature (°C)	GLC Yield (%)
1	FL11-450	450	56
2	FL11-550	550	71
3	FL11-650	650	61
4	FL11-750	750	60

temperature to 650 °C a decrease in yield to 61% was noticed. Still further increase in calcination temperature to 750 °C a marginal decrease in the yield of GLC was observed. So as to understand the difference in activity with the change in the calcination temperature the catalysts were further characterized.

3.4 Characterization of Catalysts Calcined at Different Temperatures

The XRD pattern of FL-11 catalyst calcined at different temperatures in the range of 450–750 °C is illustrated in Fig. 4. The diffraction pattern showed major reflections at 32.3° due to the presence of the LaFeO₃ phase. The FL-11 catalysts calcined at 450 °C showed a broad peak at 13.10° ascribed to the presence of La(OH)₃ phase. The predominant phase observed at all calcination temperature is LaFeO₃. The intensity of LaFeO₃ peak increased with raising in calcination temperature.

Raman spectra of the FL-11 catalysts calcined at different calcination temperatures are shown in Fig. 5. The catalyst calcined at 450–650 °C showed a broad Raman band at 630 cm⁻¹ is attributed to the presence of LaFeO₃ phase [31, 41]. However, at higher calcination temperature of 750 °C, the band position located at 154 and 179.3 cm⁻¹ are attributed to the presence of one phonon scattering that confirms the presence of La in the cationic lattice [38, 39, 42]. There are two sharp intense Raman bands observed at 222.8 cm⁻¹ (A_{1g} mode) and 291.6 cm⁻¹ (E_g mode) which

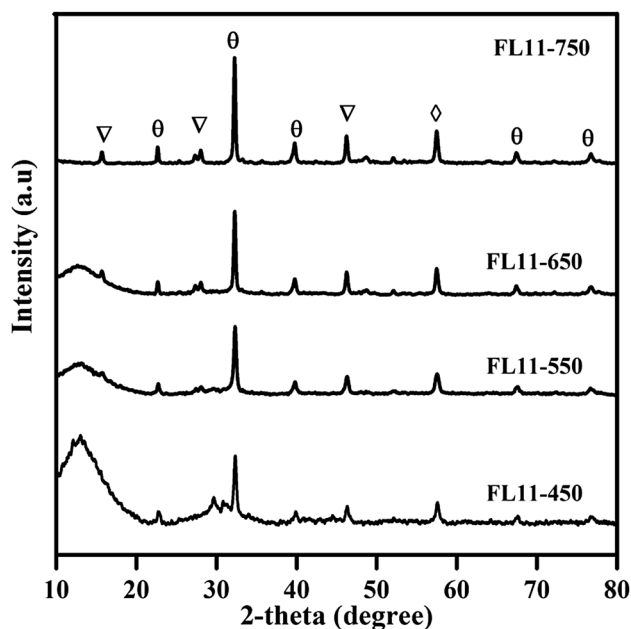


Fig. 4 X-Ray diffraction of FL-11 catalyst calcined at different calcination temperatures. La₂O₃ (filled circle), La(OH)₃ (inverted triangle), La₂O₂CO₃ (asterisk) and LaFeO₃ (open diamond)

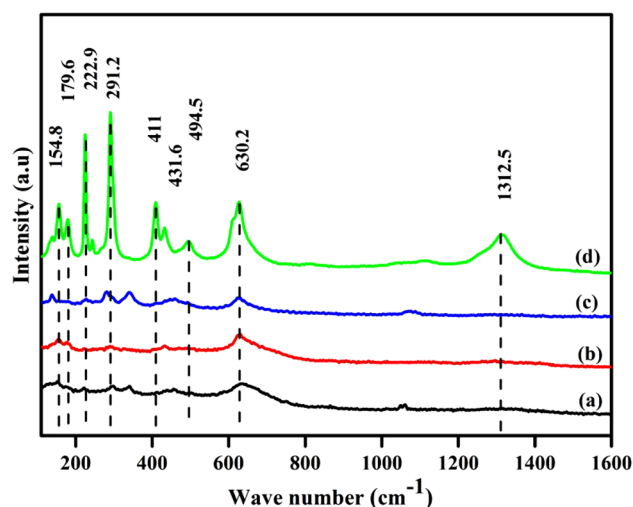


Fig. 5 Raman spectra of FL-11 catalyst calcined at (a) 450 °C, (b) 550 °C, (c) 650 °C and (d) 750 °C temperatures

are ascribed to Fe (+3) oxide phase resembles to α -Fe₂O₃ (hematite) structure [31, 32]. In addition, the broad Raman band observed at 1312.8 cm⁻¹ due to second-order scattering where IR active LO mode appeared due to combination of both Raman bands at 630 and 490 cm⁻¹ respectively [31, 43]. Thus, it is evident that upon increasing the calcination temperature of the catalyst the Raman peaks are broadened without much shifting and thus generated defects in the lattice. These defects in cationic and anionic lattice confirmed the presence of the LaFeO₃ phase which is also well agreed with XPS and XRD studies.

The acidic and basic properties of the catalysts calcined at different temperatures are estimated by TPD of NH₃ and CO₂ respectively and the results are shown in Table 5. The TPD of CO₂ and NH₃ patterns are presented in Figs. S4 and S5 respectively (Supplementary information). The catalysts calcined at 450 °C exhibited low amount of basicity and it is increased with increase in calcination temperature up to 550 °C. Further enhancement in temperature resulted in gradual decrease in the number of basic sites. In the case of acidity, the FL-11 catalyst calcined at 450 °C showed low acidity consists of weak

Table 5 Acidity and basicity of FL-11 catalysts calcined at different temperatures

S. no.	Catalysts	Basicity (mmol/g)	Acidity (mmol/g)
1	FL11-450	0.305	0.152
2	FL11-550	1.413	0.382
3	FL11-650	6.758	0.089
4	FL11-750	4.158	0.421

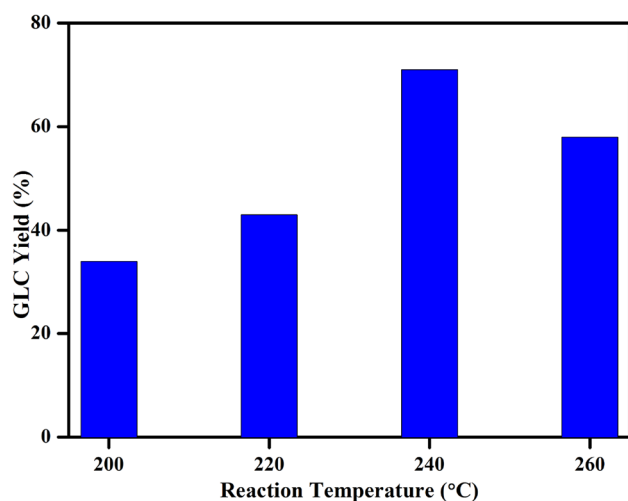


Fig. 6 The influence of reaction temperature on glycerol transesterification over FL-11 catalyst

and moderate acidic sites. The catalyst calcined at 550 °C exhibited higher amount acidity mainly associated with strong acidic sites. Further increase in the calcination temperature led to decrease in the total acidity. The catalysts calcined at above 650 °C showed the presence of both moderate and strong acidic sites.

3.5 Effect of Reaction Temperature

The influence of reaction temperature for the transesterification of glycerol over the active FL-11 catalyst calcined at 550 °C is shown in Fig. 6. The yield of GLC increased with increasing the reaction temperature from 200 to 240 °C. The highest yield of 71% of GLC achieved at the reaction temperature of 240 °C. When the reaction temperature increased from 240 to 260 °C, the amount of yield decreased to 58%. The decrease in the yield of GC at high reaction temperature is due to further conversion of GC to glycidol [44]. It is concluded that the reaction temperature of 240 °C is favourable over the FL-11 catalyst.

3.6 Effect of Glycerol to Dimethyl Carbonate Molar Ratio

In the preparation of GLC, the mole ratio of DMC to glycerol plays an important role in the transesterification reaction. The influence of the mole ratio of DMC to glycerol was studied and the results are presented in Fig. 7. As the DMC to glycerol ratio increase the rate of the reaction increased up to a mole ratio of 4. Further increase in the ratio led to a marginal decrease in the overall reaction rate. The increase in the reaction rate with more amount of DMC might be

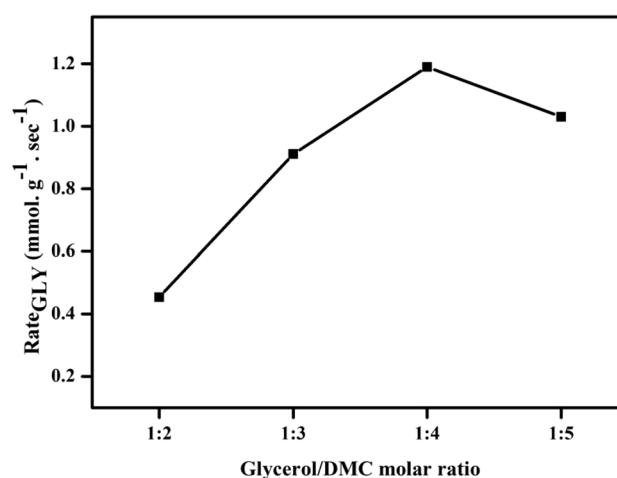


Fig. 7 The effect of glycerol to DMC ratio on glycerol transesterification over FL-11 catalyst

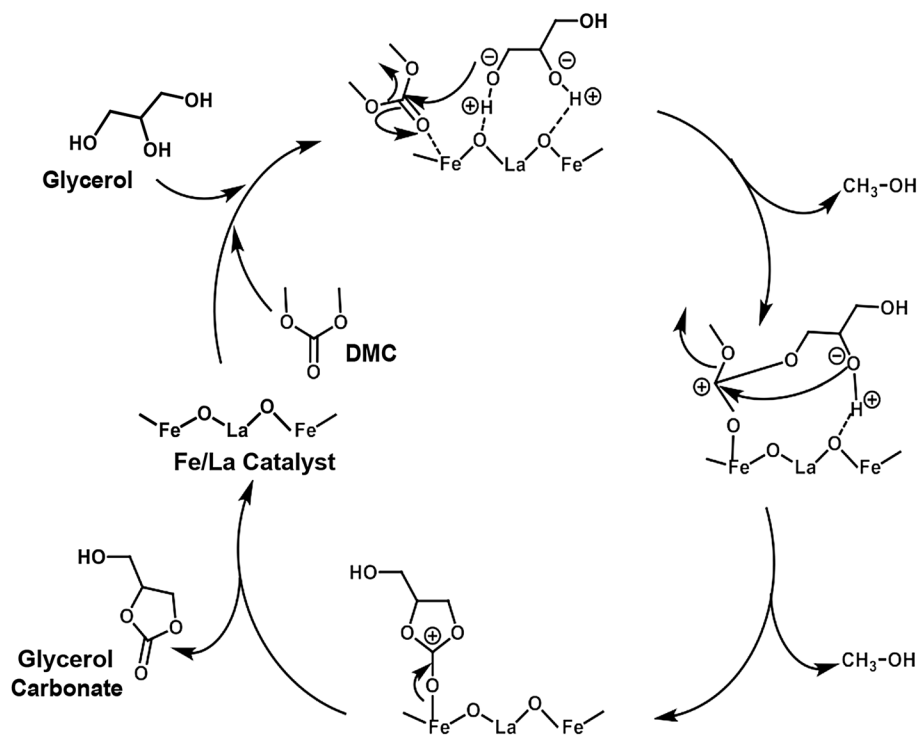
due to the more availability of the carbonating agents to glycerol. The increase in DMC concentration subsequently excels in the higher yield of GLC and reduces the formation of glycidol and at the same time inhibits the formation of other by-products [45]. It is observed that an additional increase in DMC to glycerol mole ratio to 5, the reaction rate is decreased. This might be related to blocking of active sites mostly by DMC and the number of available sites to glycerol might decrease thus lead to a decrease in overall activity.

3.7 Plausible Reaction Mechanism

Based on the nature of base and acidic sites of the catalyst and the product distribution during glycerol transesterification with DMC, a plausible reaction mechanism is proposed as shown in Scheme 1. In the reaction mechanism glycerol molecule acidic proton of hydroxyl group interacted with the Lewis basic site of the Fe–La catalyst. The other reactant DMC might adsorb on the acidic sites the catalysts associated with Fe. Then it is followed by the attack of oxygen of the glycerol hydroxyl group on the carbonyl carbon of DMC. This is followed by an elimination of the methoxy group in the form of methanol. Then, the oxygen of the secondary hydroxyl of glycerol attacks the DMC carbonyl carbon. This led to elimination of methanol followed by formation of glycerol carbonate.

3.8 Comparison of the Activity with Reported Catalysts

The transesterification of glycerol with DMC activity of the present FL-11 catalyst was compared with the reported catalysts. The comparison of activity results of the different reported catalytic systems are presented in Table 6. The

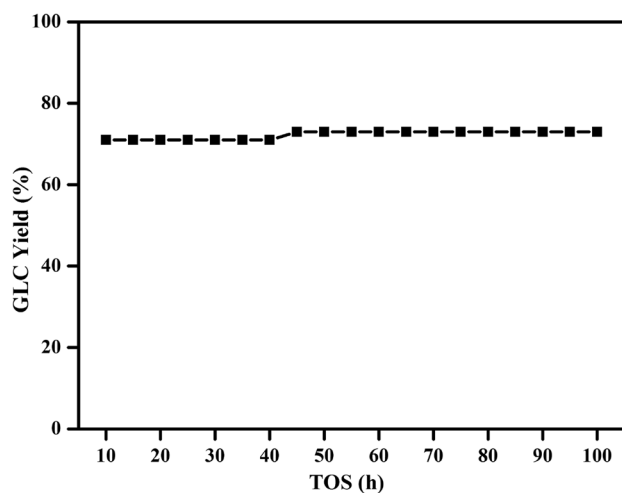
Scheme 1. Plausible reaction mechanism for glycerol transesterification with DMC**Table 6** Comparison of FL-11 catalyst activity with reported catalysts

Catalysts	Mode of operation	DMC/Glycerol (Molar ratio)	Reaction temperature (°C)	GLC yield (%)	GLC sel. (%)	TOS (h)	Reference
Ambersep 900	Flow reactor; with solvent	4:1	140	78	82	–	[20]
PS-P2-t-Bu	Flow reactor with homogeneous catalyst	3:1	135	63	84	80	[22]
CaO–ZrO ₂	Fixed bed continuous reaction	3:1	90	90	93	15	[23]
Fe–La–O	Fixed bed continuous reaction	4:1	240	71	100	100	Present work

reported continuous reactions are carried with flow reactor using both homogeneous and heterogeneous catalysts. The Ambersep-900 catalyst gave about 78% yield of GLC and the details about the catalyst stability is not reported. The other reaction used homogeneous catalyst under flow conditions with 63% conversion. Fixed bed continuous reaction is reported using CaO–ZrO₂ catalyst which showed 90% yield with limited stability up to 15 h. The present catalyst showed 71% GLC yield with a high stability of 100 h. These results indicate the superior activity and stability of FL-11 catalysts for the synthesis of GLC.

3.9 Time on Stream Analysis

The stability of the FL-11 catalyst unveiled by conducting time on stream analysis and the obtained results are shown in Fig. 8. Interestingly, it is found that the catalytic activity

**Fig. 8** Time on stream analysis of FL-11 catalyst during transesterification of glycerol with DMC

remains unchanged up to 40 h of reaction time with 71% GLC yield. Interestingly, on further progress, the yield of GLC increased marginally with TOS and continued to show a stable yield up to 100 h. It is noteworthy to mention that the FL-11 catalyst retained high stability over a period of 100 h. In comparison with the reported literature, this is the highly stable catalyst for the continuous preparation of GLC by glycerol transesterification.

In order to know the details about the stability of the FL-11 catalyst, the spent catalyst was characterized by SEM EDAX and TGA. The details of the characterization of FL-11 fresh and used catalysts are shown in Fig. S6 and 7 (Supplementary information). The SEM images (Fig. S6) suggests that there was no distinguishable difference in the morphology of the spent catalyst after 100 h of reaction. The EDAX analysis also showed similar patterns as that of virgin catalyst. The TGA profiles (Fig. S7) of the fresh and used catalysts suggests that the difference in the weight loss of fresh and used catalysts is marginal. This indicates that there was no absorption of any organic species and coke in the used catalyst. These results suggest that the FL-11 catalyst is highly stable and active for the preparation of glycerol carbonate.

4 Conclusion

In summary, Fe–La mixed oxide catalysts were prepared by co-precipitation method and evaluated for the synthesis of glycerol carbonate by continuous transesterification of glycerol with DMC. Fe–La mixed oxide catalyst with molar ratio of 1:1 exhibited the highest 71% yield of GLC. The higher activity of the catalyst is due to the presence of Fe and La mixed oxides in LaFeO₃ phase. The formation of mixed oxide phase created a greater number of strong acidic and basic sites. The catalyst surface and structural properties and there by the yield of glycerol carbonate also affected with catalyst calcination temperature. The yield of glycerol carbonate during glycerol transesterification also depends on the reaction parameters. The FL catalysts are highly stable and showed 100 h of stability with constant yield.

Acknowledgements The authors thanks CSIR, New Delhi for the financial support in the form of Mission Mode project HCP-0009. We thank Director, CSIR-IICT for permitting to publish our results (IICT Communication No: IICT/Pubs./2020-127)

References

- Fairless D (2007) Biofuel: The little shrub that could: maybe. *Nature* 449:652–655
- Schubert C (2006) Can biofuels finally take center stage? *Nat Biotechnol* 24:777–784
- Janaun J, Ellis N (2010) Perspectives on biodiesel as a sustainable fuel. *Renew Sust Energ Rev* 14:1312–1320
- Lewis P, Karimi B, Shan Y, Rasdorf W (2019) Comparing the economic, energy, and environmental impacts of biodiesel versus petroleum diesel fuel use in construction equipment. *Int J Construct Educ Res* 15:276–290
- Kim YC, Moon DJ (2019) Sustainable process for the synthesis of value-added products using glycerol as a useful raw material. *Catal Surv Asia* 23:10–22
- Anitha M, Kamarudin SK, Kofli NT (2016) The potential of glycerol as a value-added commodity. *Chem Eng J* 295:119–130
- Payormhorm J, Idem R (2020) Synthesis of C-doped TiO₂ by sol-microwave method for photocatalytic conversion of glycerol to value-added chemicals under visible light. *Appl Catal A* 590:117362
- Satgé-De Caro P, Bandres M, Urrutigoity M et al (2019) Recent progress in synthesis of glycerol carbonate and evaluation of its plasticizing properties. *Front Chem* 7:308
- Szöri M, Raj Giri B, Wang Z et al (2018) Glycerol carbonate as a fuel additive for a sustainable future. *Sustain Energy Fuels* 2:2171–2178
- Christy S, Noschese A, Lomeli-Rodriguez M et al (2018) Recent progress in the synthesis and applications of glycerol carbonate. *Curr Opin* 14:99–107
- Burk RM, Roof MB (1993) A safe and efficient method for conversion of 1,2- and 1,3-diols to cyclic carbonates utilizing triphosgene. *Tetrahedron Lett* 34:395–398
- Aresta M, Dibenedetto A, Nocito F, Pastore C (2006) A study on the carboxylation of glycerol to glycerol carbonate with carbon dioxide: the role of the catalyst, solvent and reaction conditions. *J Mol Catal A Chem* 257:149–153
- George J, Patel Y, Pillai SM, Munshi P (2009) Methanol assisted selective formation of 1,2-glycerol carbonate from glycerol and carbon dioxide using nBu₂SnO as a catalyst. *J Mol Catal A Chem* 304:1–7
- Parameswaram G, Srinivas M, Babu BH (2013) Transesterification of glycerol with dimethyl carbonate for the synthesis of glycerol carbonate over Mg/Zr/Sr mixed oxide base catalysts. *Catal Sci Technol* 3:3242–3249
- Teng WK, Ngoh GC, Yusoff R, Aroua MK (2014) A review on the performance of glycerol carbonate production via catalytic transesterification: Effects of influencing parameters. *Energ Convers Manage* 88:484–497
- Ochoa-Gómez JR, Gómez-Jiménez-Aberasturi O, Maestro-Madurga B (2009) Synthesis of glycerol carbonate from glycerol and dimethyl carbonate by transesterification: catalyst screening and reaction optimization. *Appl Catal A* 366:315–324
- Tang Y, Xue Y, Li Z (2019) Heterogeneous synthesis of glycerol carbonate from glycerol and dimethyl carbonate catalyzed by LiCl/CaO. *J Saudi Chem Soc* 23:494–502
- Pradhan G, Chandra Sharma Y (2020) Studies on green synthesis of glycerol carbonate from waste cooking oil derived glycerol over an economically viable NiMgOx heterogeneous solid base catalyst. *J. Clean. Prod.* 1:121258
- Álvarez MG, Plíšková M, Segarra AM (2012) Synthesis of glycerol carbonates by transesterification of glycerol in a continuous system using supported hydrotalcites as catalysts. *Appl Catal B Environ* 113–114:212–220
- Mileghem SV, Borggraeve WMD, Baxendale IR (2018) A robust and scalable continuous flow process for glycerol carbonate. *Chem Eng Technol* 41:2014–2023
- Nogueira DO, de Souza SP, Leão RAC (2015) Process intensification for tertiary amine catalyzed glycerol carbonate production:

- translating microwave irradiation to a continuous-flow process. *RSC Adv* 5:20945–20950
22. Wang Z, Gérardy R, Gauron G (2019) Solvent-free organocatalytic preparation of cyclic organic carbonates under scalable continuous flow conditions. *React Chem Eng* 4:17–26
 23. Zhang X, Wei S, Zhao X (2020) Preparation of mesoporous CaO-ZrO₂ catalysts without template for the continuous synthesis of glycerol carbonate in a fixed-bed reactor. *Appl Catal A-Gen* 590:117313
 24. Lari GM, de Moura ABL, Weimann L (2017) Design of a technical Mg–Al mixed oxide catalyst for the continuous manufacture of glycerol carbonate. *J Mater Chem A* 5:16200–16211
 25. Singh D, Reddy B, Ganesh A, Mahajani S (2014) Zinc/lanthanum mixed-oxide catalyst for the synthesis of glycerol carbonate by transesterification of glycerol. *Ind Eng Chem Res* 53:18786–18795
 26. Simanjuntak FSH, Widyaya VT, Kim CS (2013) Synthesis of glycerol carbonate from glycerol and dimethyl carbonate using magnesium–lanthanum mixed oxide catalyst. *Chem Eng Sci* 94:265–270
 27. Wang L, Ma Y, Wang Y, Liu S, Deng Y (2011) Efficient synthesis of glycerol carbonate from glycerol and urea with lanthanum oxide as a solid base catalyst. *Catal Commun* 12:1458–1462
 28. Ismail AA (2005) Synthesis and characterization of Y₂O₃/Fe₂O₃/TiO₂ nanoparticles by sol–gel method. *Appl Catal B Environ* 58:115–121
 29. Fleming P, Farrell RA, Holmes JD, Morris MA (2010) The rapid formation of La(OH)₃ from La₂O₃ powders on exposure to water vapor. *J Am Ceram Soc* 93:1187–1194. <https://doi.org/10.1111/j.1551-2916.2009.03564.x>
 30. Gong S, Xie Z, Li W (2019) Highly active and humidity resistive perovskite LaFeO₃ based catalysts for efficient ozone decomposition. *Appl Catal B Environ* 241:578–587
 31. Blanck D, Schön A, Mamede A-S (2017) In situ Raman spectroscopy evidence of an accessible phase potentially involved in the enhanced activity of La-deficient lanthanum orthoferrite in 3-way catalysis (TWC). *Catal Today* 283:151–157
 32. de Faria DLA, Silva SV, de Oliveira MT (1997) Raman microspectroscopy of some iron oxides and oxyhydroxides. *J Raman Spectrosc* 28:873–878
 33. Omran M, Fabritius T, Elmahdy AM (2015) XPS and FTIR spectroscopic study on microwave treated high phosphorus iron ore. *Appl Surf Sci* 345:127–140
 34. Dhinesh Kumar R, Jayavel R (2014) Facile hydrothermal synthesis and characterization of LaFeO₃ nanospheres for visible light photocatalytic applications. *J Mater Sci Mater Electron* 25:3953–3961
 35. Zhao S, Wang Li, Wang Y, Li X (2018) Hierarchically porous LaFeO₃ perovskite prepared from the pomelo peel bio-template for catalytic oxidation of NO. *J Phys Chem Solids* 116:43–49
 36. Mills P, Sullivan JL (1983) A study of the core level electrons in iron and its three oxides by means of X-ray photoelectron spectroscopy. *J Phys D Appl Phys* 16:723–732
 37. Jain S, Adeyeye AO, Chan SY, Boothroyd CB (2004) Interface properties of iron oxide films. *J Phys D Appl Phys* 37:2720–2725
 38. Thirumalairajan S, Girija K, Hebalkar NY (2013) Shape evolution of perovskite La-FeO₃ nanostructures: a systematic investigation of growth mechanism, properties and morphology dependent photocatalytic activities. *RSC Adv* 3:7549
 39. Halwidi D, Mayr-Schmölzer W, Setvin M (2018) A full monolayer of superoxide: oxygen activation on the unmodified Ca₃Ru₂O₇ (001) surface. *J Mater Chem A* 6:5703–5713
 40. Song X, Pan D, Wu Y (2018) Synthesis of glycerol carbonate over porous La-Zr based catalysts: the role of strong and super basic sites. *J Alloys Compd* 750:828–837
 41. Lee W-Y, Yun HJ, Yoon J-W (2014) Characterization and magnetic properties of La-FeO₃ nanofibers synthesized by electrospinning. *J Alloys Compd* 583:320–324
 42. Popa M (2002) Lanthanum ferrite LaFeO₃+d nanopowders obtained by the polymerizable complex method. *Solid State Ion* 154–155:437–445
 43. Andreasson J, Holmlund J, Rauer R (2008) Electron-phonon interactions in perovskites containing Fe and Cr studied by Raman scattering using oxygen-isotope and cation substitution. *Phys Rev B* 78:235103
 44. Qing Y, Lu H, Liu Y (2018) Production of glycerol carbonate using crude glycerol from biodiesel production with DBU as a catalyst. *Chin J Chem Eng* 26:1912–1919
 45. Song X, Wu Y, Cai F (2017) High-efficiency and low-cost Li/ZnO catalysts for synthesis of glycerol carbonate from glycerol transesterification: The role of Li and ZnO interaction. *Appl Catal A-Gen* 532:77–85

Publisher's Note Springer Nature remains neutral with regard to jurisdictional claims in published maps and institutional affiliations.

Affiliations

Piyusa P. Pattanaik^{1,2} · P. Mahesh Kumar^{1,2} · N. Raju¹ · N. Lingaiah^{1,2}

✉ N. Lingaiah
nakkalingaiah@iict.res.in

² Academy of Scientific and Innovative Research (AcSIR), Ghaziabad-201002, India

¹ Department of Catalysis & Fine Chemicals, CSIR-Indian Institute of Chemical Technology, Hyderabad 500 007, India